

Cite this article as: Wang Yunlei, Ren Liping, Yang Fangzhou, et al. Research Progress on Fabrication Technology and Properties of SiC Particle-Reinforced Aluminum Matrix Composites[J]. Rare Metal Materials and Engineering, 2022, 51(04): 1270-1282.

REVIEW

# Research Progress on Fabrication Technology and Properties of SiC Particle-Reinforced Aluminum Matrix Composites

Wang Yunlei<sup>1,2,3</sup>, Ren Liping<sup>1</sup>, Yang Fangzhou<sup>1</sup>, Liu Qi<sup>2</sup>, Cao Yu<sup>3</sup>, Luo Hongwei<sup>4</sup>

<sup>1</sup> College of Materials Science and Engineering, Chongqing University of Arts and Sciences, Chongqing 402160, China; <sup>2</sup> National Instrument Functional Materials Engineering and Technology Research Center, Chongqing Materials Research Institute Co., Ltd, Chongqing 400707, China; <sup>3</sup> College of Materials Science and Engineering, Chongqing University, Chongqing 400044, China; <sup>4</sup> Department of Technical Research and Development, Chongqing Bairuike New Material Technology Co., Ltd, Chongqing 402560, China

**Abstract:** SiC particle-reinforced aluminum matrix composites have high specific strength, high specific modulus, high wear resistance, and excellent corrosion resistance, which are one of the best materials for replacing traditional steel due to the lightweight design they offer in mechanical structures. They have broad application prospects in the automotive, machinery, aviation, and electronic packaging fields. Therefore, they have received much attention from scientific research workers in all fields. This research summarized the fabrication technology, properties, and reinforcement mechanisms of SiC particle-reinforced aluminum matrix composites, and discussed the technical difficulties and improvements in the preparation of these composites. Finally, the research and applications of SiC particle-reinforced aluminum composites were summarized.

**Key words:** SiC particles; aluminum matrix composites; fabrication technology; reinforcement mechanism

Aluminum (Al) is a light and active metal material with a density of 2.702 g/cm<sup>3</sup>, a melting point of 660 °C, and a boiling point of 2327 °C. Most of aluminum in nature is found in the form of aluminum silicate ore. Because aluminum alloy has high strength (close to or greater than that of high-quality steel) and good plasticity, it can be processed into various profiles with excellent electrical conductivity, thermal conductivity, and corrosion resistance. Therefore, aluminium alloy is the best material for replacing traditional steel due to its lightweight design in mechanical structures<sup>[1-6]</sup>. SiC particle-reinforced aluminum matrix (SiC<sub>p</sub>/Al) composites have high specific strength, high specific modulus, high wear resistance, and excellent corrosion resistance<sup>[7]</sup>. Due to these properties, they are widely used in the aerospace, shipbuilding, automotive, construction, military, internal combustion engine, and electronic packaging industries, etc. Fig. 1 demonstrates typical applications of SiC<sub>p</sub>/Al composites<sup>[11-15]</sup>.

The attractive physical and mechanical properties of metal matrix composites (MMCs), such as high specific modulus,

strength, and thermal stability, have been documented extensively. MMCs combine metallic properties (ductility and toughness) with ceramic properties (high strength and modulus), which creates greater strength in shear and compression and higher service temperature capabilities<sup>[13-15]</sup>. Reinforcement materials<sup>[16,17]</sup> include carbides (e.g., SiC, B<sub>4</sub>C), nitrides (e.g., Si<sub>3</sub>N<sub>4</sub>, AlN), oxides (e.g., Al<sub>2</sub>O<sub>3</sub>, SiO<sub>2</sub>), and elemental materials (e.g., C, Si). The reinforcements may be in the form of continuous fibers, chopped fibers, whiskers, platelets, or particulates. SiC, for example, is used in aluminum and magnesium MMCs in all of the above-mentioned forms, and carbon and silicon fibers are used in aluminum-, magnesium-, and copper-matrix composites.

Currently, the methods for preparing SiC/Al composites include the semi-solid stirring melting casting method<sup>[18-25]</sup>, melt infiltration method<sup>[26-30]</sup>, powder metallurgy method<sup>[31-33]</sup>, jet deposition method, and pulse current sintering method<sup>[34,35]</sup>. The commonest method is the semi-solid stirring melting casting method, which has a short process and low cost and

Received date: September 23, 2021

Foundation item: High-level Talent Introduction Program for Chongqing University of Arts and Sciences (2017RCH01); Science and Technology Research Program of Chongqing Municipal Education Commission (KJQN202001301); Industry-University-Research Cooperation Program (WLHX-2020-0048)

Corresponding author: Wang Yunlei, Ph. D., Lecturer, School of Materials Science and Engineering, Chongqing University of Arts and Sciences, Chongqing 402160, P. R. China, Tel: 0086-23-49855073, E-mail: wangyunlei@cqu.edu.cn

Copyright © 2022, Northwest Institute for Nonferrous Metal Research. Published by Science Press. All rights reserved.

can produce materials of various complex shapes, and has broad application prospects.

Although they are still in the development stage, SiC/Al composites<sup>[36-44]</sup> have been studied for more than 50 years, during which the American scholar Logsdon<sup>[36]</sup> proposed the preparation and development of MMCs in non-long-fiber reinforcement, especially in SiC<sub>w</sub>-(SiC whisker) and SiC<sub>p</sub>-(SiC particle) reinforced MMCs. With the development of fabrication technology, Myriounis<sup>[42]</sup> proposed a model for dynamical prediction of SiC particle segregation and interfacial strength behavior in order to study the micromechanical properties of SiC/Al composites.

## 1 Preparation Methods and Characteristics of SiC<sub>p</sub>/Al Composites

SiC<sub>p</sub>/Al composites are reinforced using SiC and Al<sub>2</sub>O<sub>3</sub> ceramic particles, which are mixed with the aluminum matrix to form a new composite. The composite has high wear resistance, high hardness and strength, good thermal

conductivity, low thermal expansion coefficient, and excellent corrosion resistance. These properties make it the best choice for light weight aluminum to replace cast iron when designing and manufacturing automobile brake disc material. SiC<sub>p</sub>/Al composites are usually prepared by stirring casting, melt infiltration, powder metallurgy, jet deposition, or pulse current sintering (Fig. 2). The melt infiltration method includes both the pressure infiltration method and pressureless infiltration method.

Researchers have also developed additional processes for preparing SiC<sub>p</sub>/Al composites. For example, Alizade et al<sup>[45]</sup> prepared nano-SiC<sub>p</sub>/Al composites with excellent comprehensive mechanical properties through accumulative roll bonding (ARB). Sahin et al<sup>[46]</sup> prepared SiC<sub>p</sub>/Al composites with different volume fractions using the vacuum infiltration method, and studied the effects of different SiC particle volume fractions on the microstructure and properties of SiC<sub>p</sub>/Al composites to determine the optimal volume fraction.

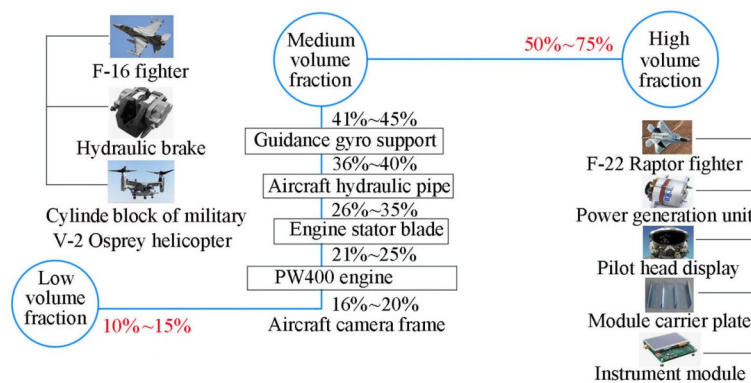


Fig.1 Typical applications of SiC<sub>p</sub>/Al composites<sup>[11-15]</sup>

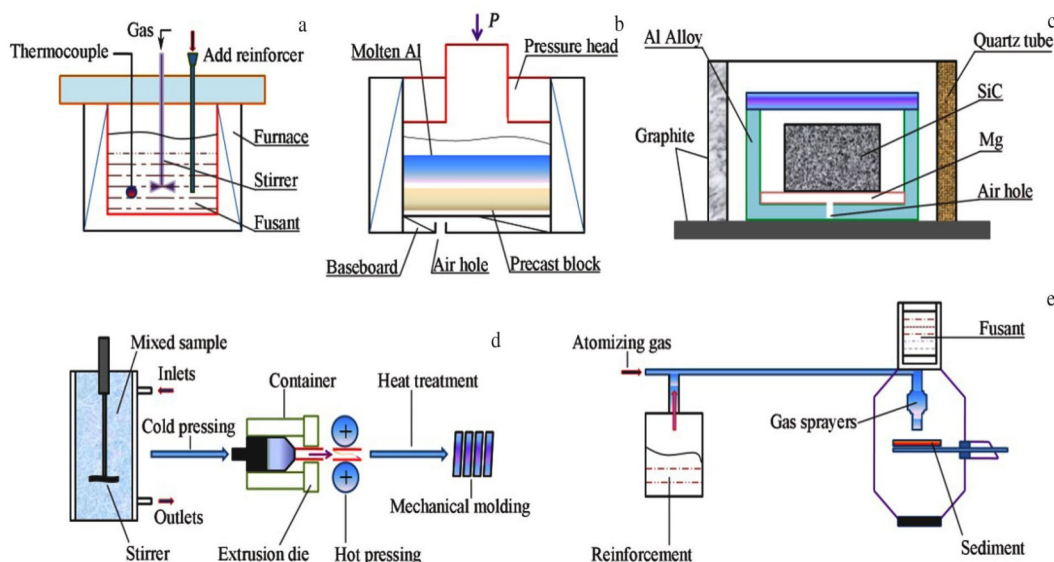


Fig.2 Five representative fabrication routes for SiC particle-reinforced aluminum matrix composites: (a) stirring casting, (b) pressure infiltration, (c) pressure-less infiltration, (d) powder metallurgy, and (e) jet deposition<sup>[16-33]</sup>

## 1.1 Stirring casting method

The semi-solid stirring casting process combines SiC and aluminum through mechanical mixing to maximize the effect of the SiC particles by distributing them evenly in the aluminum substrate, forming a good interface, creating homogeneity, and refining the grain size of the composite materials. This allows the SiC<sub>p</sub>/Al composites to achieve the best performance possible. The semi-solid stirring temperature is generally controlled at 595~610 °C. The SiC particles are washed with clean water and then coarsened with 36% hydrochloric acid. Then, the particles are heated to 950 °C in a box-resistance furnace for 4 h. The purpose of this method is to remove the gas and water vapor adsorbed on the surface of the SiC particles, reduce the particle agglomeration as much as possible, and increase the fluidity of the SiC particles and the mutual wettability between the SiC particles and the matrix. This allows them to be distributed evenly throughout the matrix.

The stirring smelting casting method has the advantages of simple process and low cost. Furthermore, it can produce composite materials with more complex shapes, so it has broad application prospects. However, this method also has some weaknesses, such as poor mutual wettability between SiC particles and liquid aluminum, difficulty in particle addition, poor uniformity and dispersion, and easy chemical reaction at the interface. These weaknesses limit its potential applications.

### 1.1.1 Effects of agitators on the distribution of SiC particles

In the stirring casting method, liquid stirring can lead to some problems, such as poor wettability between particles and liquid aluminum as well as difficulty for the particles to enter the liquid aluminum. Semi-solid stirring method can overcome the poor wettability of particles and liquid aluminum and achieve easy preparation of composite materials with uniform particle distribution. However, the fluidity of the composite materials prepared by semi-solid stirring is worse than that prepared by liquid stirring, as the agglomeration of particles reduces the fluidity of the melt.

Therefore, the flow behavior of the melt becomes the key determinant for the uniform distribution of particles in the Al matrix.

Mao et al.<sup>[47]</sup> conducted a numerical simulation study on the flow field and velocity field characteristics of a composite agitator by combining numerical simulation with experimental research (Fig. 3). They designed different stirrers, including four-bladed paddle, three-bladed propeller, and double-stage three-bladed screw propeller, to stir SiC<sub>p</sub>/Al composites. By comparing the simulation and microstructure observation, they found that the four-bladed paddle did not form a good, single-blade suction channel and did not fully enter the melt particles. The three-bladed propeller produced a composite particle reunion phenomenon, axial and radial velocities of stirring flow field with double-stage three-bladed screw propeller were both large, and a negative pressure channel was formed in the pressure field. Furthermore, the stirring range was wide, which can form composite materials with uniform particle distribution.

### 1.1.2 Effect of stirring temperature on the distribution of SiC particles

Bai et al.<sup>[48]</sup> selected four temperatures within 595~650 °C for their stirring experiment. The semi-solid stirring temperature range was set at 595~610 °C, and the liquid stirring temperature range was set at 610 °C to 650 °C. Fig.4 shows the microstructure of the SiC particle distribution at the four different stirring temperatures. The semi-solid stirring produces a higher melt viscosity because of the collision between the primary phase of  $\alpha$ -aluminum and the SiC clusters and the resultant friction. This promotes the particle dispersion, as the internal friction crushes the particle cluster and creates greater shear force to ensure the uniform dispersion of the SiC. As seen in Fig.4b, the uniformity is best at a mixing temperature of 610 °C. Fig.4c and 4d show the deterioration of the SiC particle dispersion due to the liquid agitation caused by the disappearance of both the grinding and the effect of primary  $\alpha$ -aluminum on the agglomeration of the SiC particles. Furthermore, due to the decrease of the overall

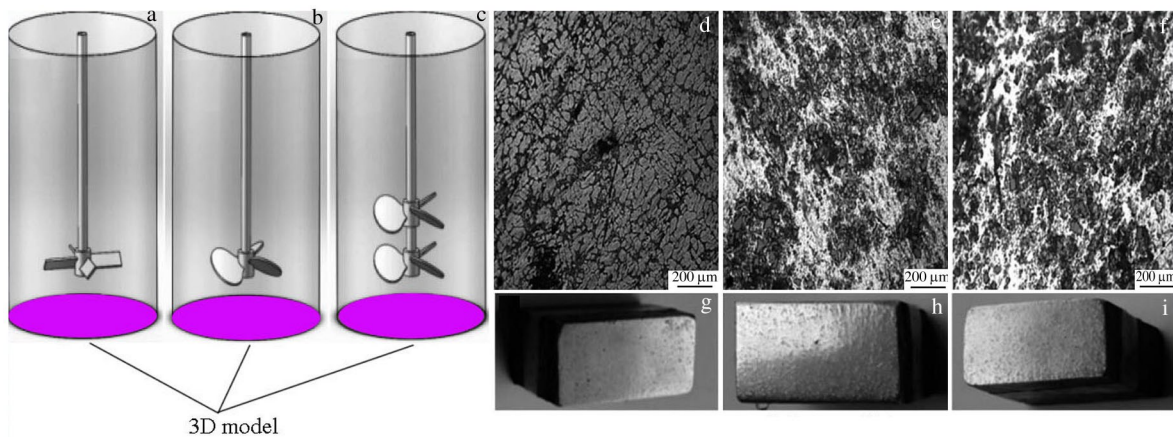


Fig.3 3D modeling (a~c) and microstructures (d~f) and corresponding macromorphologies (g~i): (a, d, g) four-bladed paddle, (b, e, h) three-bladed propeller, and (c, f, i) double-stage three-bladed screw propeller

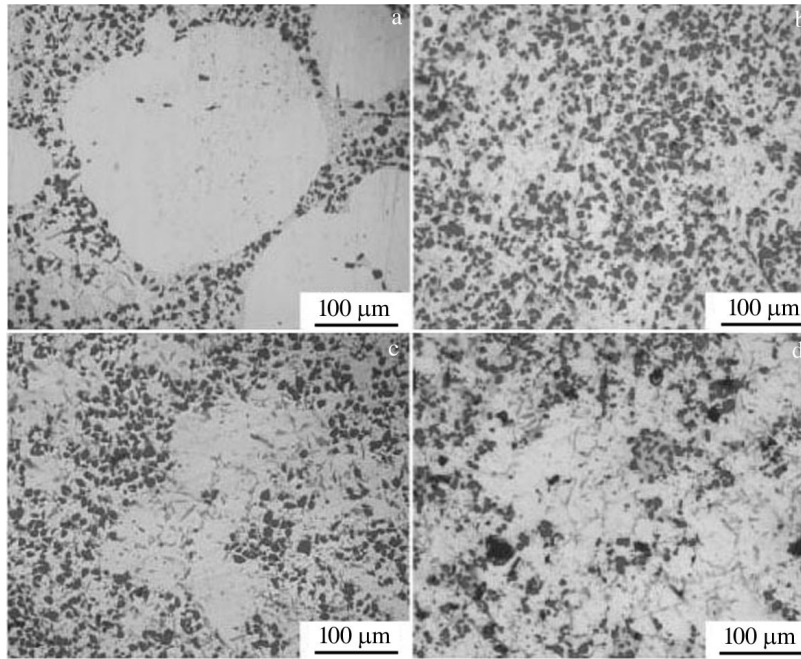


Fig.4 Effect of stirring temperature on the distribution of SiC particles in the composites: (a) 595 °C, (b) 610 °C, (c) 630 °C, and (d) 650 °C<sup>[48]</sup>

mixture viscosity, the SiC particles are prone to sedimentation, which prevents uniform dispersion.

#### 1.1.3 Effect of stirring speed on the distribution of SiC particles

For semi-solid stirring, Bai et al<sup>[48]</sup> studied the effect of stirring speeds of 200, 500, 650 and 800 r/min on the distribution of SiC particles. They found that the SiC particle agglomeration was difficult to disperse at 200 r/min (Fig. 5a)

due to the insufficient shearing force of the melt. Thus, the distribution of the SiC particles was not uniform, which led to the existence of a large number of microscopic pores in the composites. When the stirring speed was increased to 500 r/min, the agglomeration of the SiC particles was weakened, and the microscopic pores were also reduced. Thus, with the increase of stirring speed, the impact of the frequency and velocity of primary  $\alpha$ -aluminum particles on the SiC particles

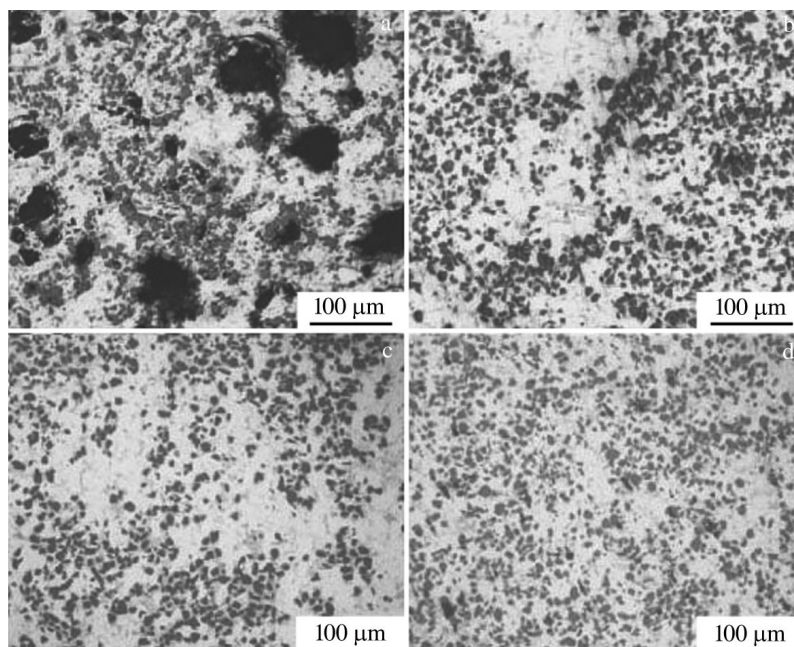


Fig.5 Effect of stirring speed on the distribution of SiC particles in composites prepared by semi-solid stirring: (a) 200 r/min, (b) 500 r/min, (c) 650 r/min and (d) 800 r/min<sup>[48]</sup>

in the matrix will increase, and the velocity and pressure difference in the melt will increase accordingly. This will improve the uniform distribution of the SiC particles, because the increase of shear force significantly reduces the agglomeration of the SiC particles and improves the homogeneity of the microstructure. As the stirring speed increased to 650 r/min (Fig. 5c), the shearing force increased, and the microstructure uniformity continued to increase. The stirring shearing force reached the maximum and the microstructure uniformity was the best at a stirring speed of 800 r/min (Fig. 5d)

#### 1.1.4 Effect of stirring time on the distribution of SiC particles

To study the influence of stirring time on the distribution of SiC particles, the optimal stirring temperature was selected as 610 °C, and the stirring speed was set at 800 r/min. During the stirring process, the mixing of particles inside the melt consisted of two processes: “macro mixing” and “micro mixing”<sup>[49]</sup>. “Macro mixing” is the process of destroying the agglomeration of SiC particles, while “micro mixing” is the process of diffusing the SiC particles. When the macro mixing process is completed, the stirring time must be extended to destroy the agglomeration of the particles.

As shown in Fig. 6c, the dispersion uniformity of the SiC particles is best when the stirring time is 20 min. This is because the dispersion of particles in the melt is gradually realized with an extended stirring time. However, the stirring time should not be too long. As shown in Fig. 6e, the dispersion uniformity of the SiC particles decreases over time. The low melting point of Mg in the matrix alloy makes it easy to burn, which is not conducive to the wetting between the SiC particles and the matrix. Therefore, when the particles are evenly dispersed, prolonging the stirring time has a negative effect on their dispersion.

### 1.2 Melt infiltration method

The melt infiltration method is generally divided into the pressure infiltration method and pressure-less infiltration method.

#### 1.2.1 Pressure infiltration method

The pressure infiltration method is used to prepare SiC

particles by first preparing the prefabricated blocks and then placing them into the extrusion die. The die is then preheated to a certain temperature, and the aluminum alloy liquid is poured into the die. The alloy liquid infiltrates the prefabricated block to obtain the required composite material (Fig. 2b).

Liao et al<sup>[26]</sup> prepared three-dimensional (3D) porous-frame  $C_f/SiC_p$ -Al composites using the vacuum pressure infiltration method. The compressive strength of the composites increased from 168~445 MPa, and the performance was greatly improved. Maleki et al<sup>[30]</sup> synthesized SiC/Al 6061 composites with a high volume fraction of SiC using the pressure infiltration method, and their compressive strength and hardness were improved to the maximum extent.

#### 1.2.2 Pressure-less infiltration method

In the pressure-less infiltration method, preformed SiC particles and aluminum alloy are placed in a heating furnace with flowing nitrogen, and the matrix alloy is melted. The melted alloy liquid is then spontaneously infiltrated into the preformed, networked reinforcement material to form the composite material (Fig. 2c).

Yang et al<sup>[27]</sup> prepared and characterized AZ91/SiC composites using the pressure-less infiltration method. They found that indispensable conditions for the preparation of composites with excellent performance were temperature, time, and atmosphere. Additionally, they studied the second-phase particles and the particles strengthening mechanisms in detail. The phases of MgO,  $MgAl_2O_4$ ,  $Al_{12}Mg_{17}$ , and AlN were found in the composites.

### 1.3 Powder metallurgy process

Powder metallurgy is a common method used to prepare MMCs. Generally, it involves three steps: mixing, forming, and sintering (Fig. 2d). The general mixing methods include mechanical ball milling and artificial mixing. The main forming methods are molding, hot pressing, cold pressing, hot isostatic pressing, etc. Based on the research<sup>[31-33]</sup>, the two commonest powder metallurgy process routes are as follows: (1) cold pressing after mixing, followed by ordinary sintering and hot extrusion; (2) mixing the material directly after vacuum hot-pressing forming.

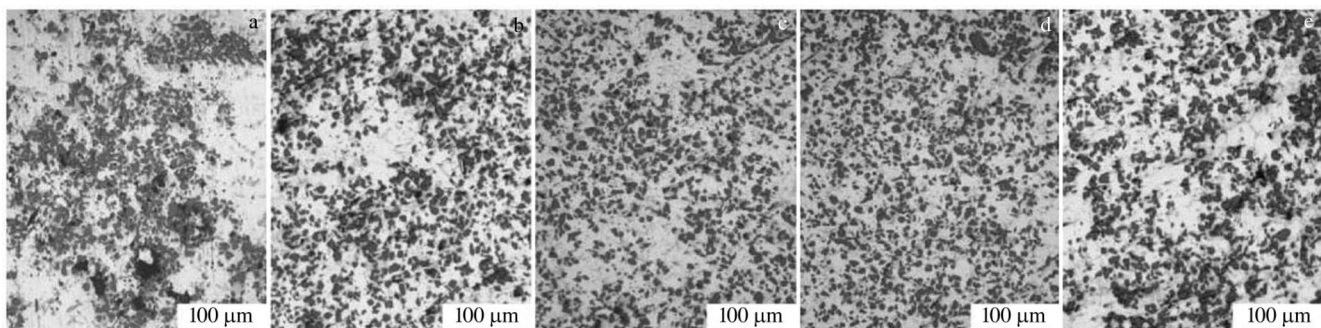


Fig.6 Effect of stirring time on the distribution of SiC particles in composites by semi-solid stirring at 610 °C and 800 r/min: (a) 10 min, (b) 15 min, (c) 20 min, (d) 25 min, and (e) 30 min<sup>[48]</sup>

## 1.4 Jet deposition

The jet deposition method atomizes the alloy liquid with a high pressure inert gas jet, which is used to spray the reinforcing phase into the alloy liquid flow. After mixing, the alloy liquid is sprayed onto the substrate and solidified rapidly (Fig. 2e). The volume fraction and particle size of the reinforcement required for the jet deposition process are not limited, the interface reaction is less, and the interface bonding strength is high. However, the equipment is expensive, and the particle utilization rate of the reinforcement is low.

To determine the microstructure and mechanical properties of  $\text{SiC}_p/\text{Al}$  composites, Gao et al.<sup>[50]</sup> used spray co-deposition technology to prepare the rolled composites with fine and uniform microstructure. Many second phase particles exist in the matrix, mainly  $\text{Al}_2\text{CuMg}$  and  $\text{Al}_2\text{Cu}$ . Sun et al.<sup>[51,52]</sup> found that the tensile flow stress of the composite sheet decreased as the deformation temperature increased, while the elongation of composite increased.

## 1.5 Pulsed current sintering

Pulsed current sintering devices include plasma activation sintering (PAS) devices and spark plasma sintering (SPS) devices, as shown in Fig. 7. The devices are composed of a pulse current, DC generator, vacuum system, pressure system, cooling system, control system, and automatic recording. The SPS device and its sintering process are similar to those of the PAS, but the SPS device only uses pulse current with a pulse gap of 12/2 ms as a power source.

Yang et al.<sup>[34,35]</sup> prepared and studied  $\text{SiC}_p/\text{Al}$  composites with a volume fraction of 33%~63% using pulsed current discharge sintering. They found that temperature and pressure

are the key factors of sintering and that only good control of sintering temperature and pressure can produce evenly distributed  $\text{SiC}$  particles.

## 2 Properties of $\text{SiC}_p/\text{Al}$ Composites

### 2.1 Mechanical properties of $\text{SiC}_p/\text{Al}$ composites

Table 1 compares the tensile properties of  $\text{SiC}_p/\text{ZL109}$  composites and ZL109 alloy at room temperature<sup>[53]</sup>. The  $\text{SiC}_p/\text{ZL109}$  composites have better yield strength and tensile strength. The yield strength increases from 256 to 305 MPa, and the tensile strength increases from 296 to 324 MPa. Additionally, the elongation decreases. The strength of the  $\text{SiC}_p/\text{ZL109}$  composites is obviously improved compared to that of the ZL109 alloy due to the strengthening effect of the dispersion of  $\text{SiC}$  particles.

To study the related mechanical properties of  $\text{SiC}_p/\text{Al}$  composites, Tokaji et al.<sup>[54]</sup> found that the size of  $\text{SiC}$  particles has an important effect on fatigue strength. Fatigue strength decreases with the increase of particle size. Yield strength and elongation also decrease (Table 2). Thus, the size and distribution of  $\text{SiC}$  particles have a corresponding influence on the mechanical properties and microstructure of materials<sup>[36,37-39]</sup>.

Ibrahim<sup>[1]</sup> studied the mechanical properties of  $\text{SiC}$ -reinforced A356 aluminum alloy under different  $\text{SiC}$  volume fractions. As seen in Table 3, the initial yield strength of the A356 aluminum alloy is 200 MPa, the ultimate tensile strength is 276 MPa, the elongation is 6%, the modulus is 75 GPa, and the density is  $2.68 \text{ g}\cdot\text{cm}^{-3}$ . When the volume fraction of the  $\text{SiC}$  particles increases, the yield strength, ultimate tensile strength, and modulus of the A356 aluminum alloy all

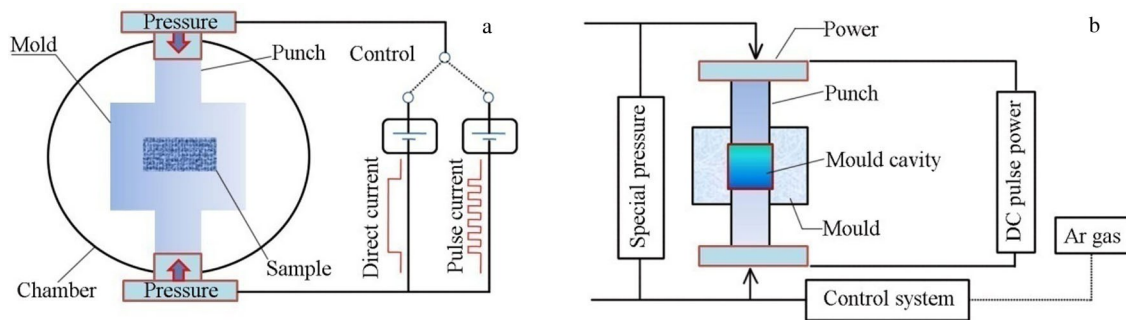


Fig.7 Schematic of pulsed current sintering device: (a) plasma activation sintering structure (PAS) and (b) spark plasma sintering structure (SPS)<sup>[34,35]</sup>

Table 1 Comparison of tensile properties at room temperature for  $\text{SiC}_p/\text{ZL109}$  composite and ZL109 alloy<sup>[53]</sup>

Material	Yield strength, $\sigma_{0.2}/\text{MPa}$	Tensile strength, $\sigma_b/\text{MPa}$	Elongation, $\delta/\%$
ZL109	256	296	3.0
$\text{SiC}_p5\%/\text{ZL109}$	293	316	1.7
$\text{SiC}_p10\%/\text{ZL109}$	305	324	0.4

increase, while the elongation decreases.

### 2.2 Machining properties of $\text{SiC}_p/\text{Al}$ composites

The mesoscopic finite element analysis (FEA) model for cutting particle-reinforced composites is shown in Fig. 8<sup>[55]</sup>. The diameter of the spherical particle is  $20 \mu\text{m}$ , and the volume fraction of the  $\text{SiC}$  particle in the composites is 30%. The workpiece length and height are 1.2 and 0.6 mm, respectively. The rake angle, relief angle, and edge radius of the diamond tool are  $5^\circ$ ,  $10^\circ$ , and  $1.5 \mu\text{m}$ , respectively. A

**Table 2 Tensile properties of unreinforced alloy and SiC<sub>p</sub>/Al composites** [54]

Alloy	Yield strength, $\sigma_{0.2}$ /MPa	Tensile strength, $\sigma_b$ /MPa	Elongation, $\delta$ /%	Reduction of area, $\psi$ /%	Elastic modulus, $E$ /GPa
Unreinforced	373	454	9	26	61
5 $\mu\text{m}$ SiC <sub>p</sub> /Al	365	462	5	8	71
20 $\mu\text{m}$ SiC <sub>p</sub> /Al	357	479	6	10	70
60 $\mu\text{m}$ SiC <sub>p</sub> /Al	356	452	4	8	72

**Table 3 Mechanical and physical properties of SiC/Al alloy composites** [11]

Alloy	Yield strength/MPa	Ultimate strength/MPa	Elongation/%	Modulus/GPa	Density/g·cm <sup>-3</sup>
A356	200	276	6.0	75	2.68
A356-10%SiC	283	303	0.6	81	-
A356-15%SiC	324	331	0.3	90	2.76
A356-20%SiC	331	352	0.4	97	-

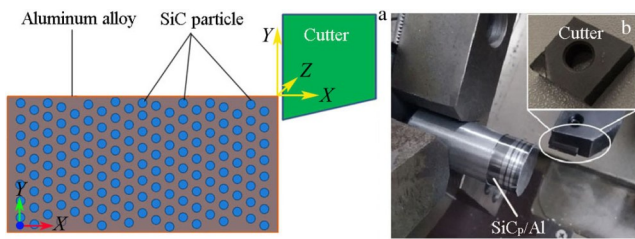


Fig.8 Simulation model (a) and experiment setup (b) for the cutting of SiC<sub>p</sub>/Al composites [55]

polycrystalline diamond (PCD) was adopted in the cutting experiments. In this study, a two-dimensional (2D) finite micro-structure-based element model was developed to simulate the orthogonal cutting of aluminum MMCs reinforced with SiC particles. The model of the workpiece was generated using a custom subroutine, which enabled random distribution of the particles in the matrix.

The effect of the milling tool nose must be considered when the axial depth of the cut is on the same size level as the tool nose radius, as the tool's effective cutting edge is mainly concentrated on the circle-shaped nose edge. Fig.9<sup>[56]</sup> shows the surface generation during the end milling process. Fig.9a demonstrates the macro picture of the end milling process. The milled surface is generated by the rotation and feed movement of the tool. Fig.9b demonstrates the micro picture

of the milling process around the tool nose. A sectional view (M-M image) is drawn as well to show the actual cutting process. The round milling path is simplified as a straight cutting path since the path can be assumed to be straight when a small area is analyzed by a microscope with high magnification. All 2D simulation models are based on the M-M image.

In order to have a deeper understanding of its cutting process, simulations are performed for cutting round particle model and polygonal particle model, and chip formation of each model at four different cutting time are shown in Fig.10<sup>[57]</sup>. As for the chip morphology, due to the high volume fraction of the SiC particle, discontinuous chips form and some SiC particles are even totally deboned from the chip.

Von Mises stress distribution shows that the stress in SiC particles is much higher than that in Al matrix. The results show that the hard SiC particles mainly bear the load during milling, while the aluminum matrix mainly transmits the load. In the aspect of machining surface morphology, the simulated cutting surface is rough, including cavity defects of different sizes.

A single flute mono crystalline diamond square end mill was used as the cutting tool. Mono crystalline diamond is considered the ideal cutting tool material due to its extreme hardness and sharpness. As shown in Fig. 11a, a mono crystalline diamond is brazed on the carbide tool shank with

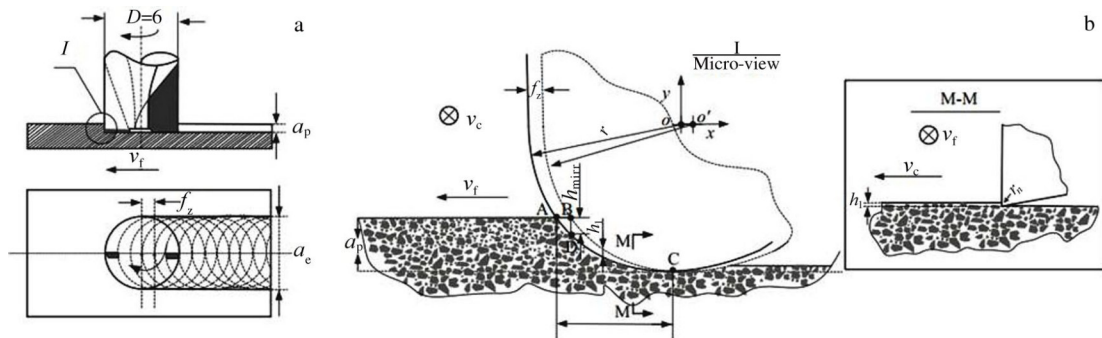


Fig.9 Schematic of surface generation during the end milling process: (a) macro picture and (b) micro picture [56]

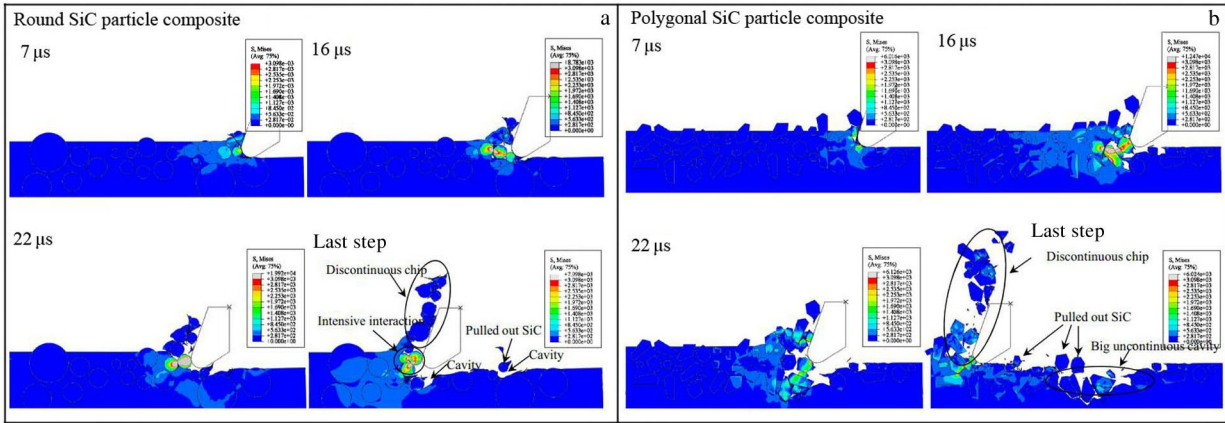


Fig.10 Cutting simulation of SiC particle composite without SiC fracture: (a) round SiC particle and (b) polygonal SiC particle<sup>[57]</sup>

an offset to form a single cutting edge. The tool diameter is about 3 mm. The cutting edge is processed to be very sharp, and the quality of the cutting edge is checked by a Leica DVM5000 microscope. The radius of the cutting edge is measured to be smaller than 0.7 μm (Fig. 11b), and the rake angle and relief angle of the cutting edge are about 0° and 5°, respectively. Fig. 11c shows a scanning electron microscopy (SEM) image of the sharp tool tip.

A workpiece sample was stuck to an iron block, which was clamped by paraffin wax. The vise is fixed on a piezoelectric dynamometer with screws so that the grinding forces  $F_a$  in the axial direction and  $F_r$  in the feed direction can be properly measured, as shown in Fig.12<sup>[59]</sup>. To eliminate the effect of the

coolant on the grinding force measurement, the grinding experiment was performed first with the coolant at the zero cutting depth of  $a_p$ . The actual grinding forces were then obtained by subtracting the grinding forces recorded during air grinding from the total grinding forces.

The SEM morphology in Fig. 12c show the surface topography of the SiC<sub>p</sub>/Al composites after ultrasonically assisted grinding (UAG). The ratio of the fracture area (marked with black color in Fig.12) on the surface after UAG is slightly higher (16.8%) than that (13.3%) after conventional grinding (CG). The SiC<sub>p</sub>/Al surface after grinding consists of three different areas: (1) the smooth area, (2) the smeared area, and (3) the fractured area.

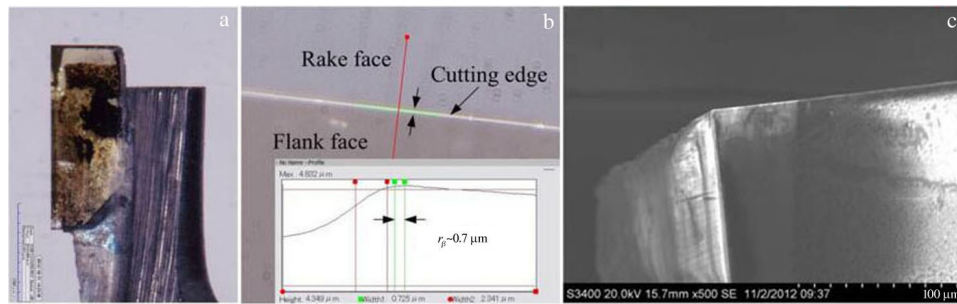


Fig.11 Single flute diamond square end mill: (a) overview of diamond flute, (b) cutting edge radius estimation, and (c) SEM image of the tool tip<sup>[58]</sup>

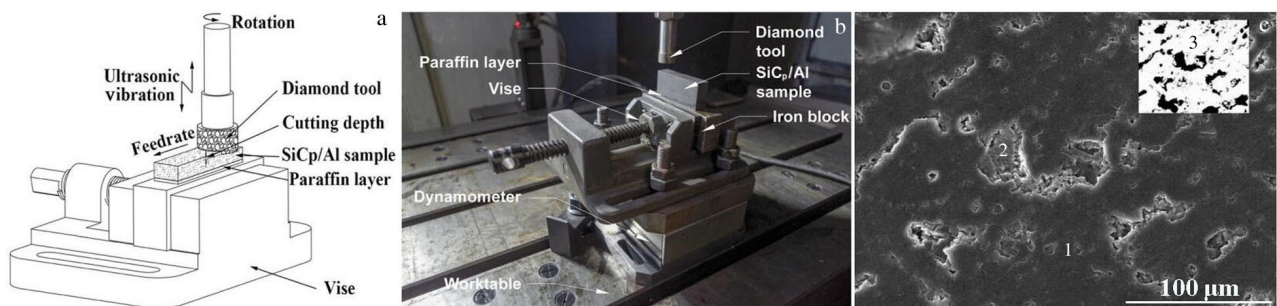


Fig.12 Schematic (a) and experimental setup (b) of UAG using a diamond grinding wheel; (c) SEM image of surface morphology of SiC<sub>p</sub>/Al after UAG<sup>[59]</sup>

### 3 Strengthening Mechanisms

#### 3.1 Spatial distribution and configuration of the reinforcement phase

The spatial distribution and configuration of the reinforcement phase are important factors for the mechanical properties that must be studied. An increasing number of scholars have studied enhanced particle non-uniform distribution in MMCs, and high-performance MMCs with the current configuration strength has become an important topic of research. To control different scales of spatial distribution and configuration of the reinforced phase in the matrix, a series of composites containing different reinforced phase configurations of the composite materials were prepared.

Huang et al.<sup>[60]</sup> systematically summarized several configurations of a metal matrix. As shown in Fig.13, the distribution of four reinforcement phases is not uniform at the micro scale, but uniform at the macro scale. The local volume fraction ( $V_L$ ) of the enhancer ranges from 0% to a specific value ( $V_{L1}$ ) in the poor enhancement region, and the local volume fraction ( $V_{L2}$ ) of the enhancer in the rich region is higher than  $V_{L1}$ , or even higher than 100%.

#### 3.2 Strengthening and toughening mechanisms of the reinforcement phase

##### 3.2.1 Fine-grain reinforcement mechanism

The introduction of reinforcing particles can cut the matrix grains to reduce their size and can also fix the matrix grain boundaries to restrict their growth. Since the grain boundaries have an inhibiting effect on dislocations, the matrix grain size directly affects the overall strength of the composite. Generally, the finer the matrix grains, the higher their

contribution to the overall strength of the composite. The number of grain boundaries can be increased by refining grain size, which can also better hinder dislocation and improve material strength. The relationship between grain size and metal material strength is determined by the Hall-Petch equation<sup>[61]</sup>:

$$\sigma_{HP} = \sigma_0 + k/D^{1/2} \quad (1)$$

where  $\sigma_{HP}$  is the yield strength,  $\sigma_0$  is a constant,  $D$  is the average grain size, and  $k$  is the strengthening factor related to the material.

##### 3.2.2 Orowan reinforcement mechanism

Orowan strengthening is caused by the interaction between the second-phase particles and dislocations. Due to the effect of loads, dislocation after the second phase is blocked. When hard particles in the second phase is hard to deform, dislocation will continue to campaign around the second phase. Hard particles will form around the dislocation loop with the second phase of the dislocation line, so the more dislocation loop is left, the stronger the effect. The reinforcement caused by the Orowan reinforcement mechanism is expressed by the following formula<sup>[62]</sup>:

$$\sigma_{OR} = \frac{0.4MG_m b}{\sqrt{2/3} \pi d_p V_p} \quad (2)$$

where  $\sigma_{OR}$  is the yield strength generated by Orowan strengthening,  $M$  is the Taylor factor,  $G_m$  is the shear modulus of the aluminum matrix,  $b$  is the Burgers vector of the dislocation,  $d_p$  is the average diameter of the second-phase particles, and  $V_p$  is the volume fraction of the second phase.

Huo et al.<sup>[63]</sup> studied the dislocation proliferation and packing manifested when the Orowan strengthening mechanism was used to prepare SiC<sub>p</sub>/Al composites (Fig.14).

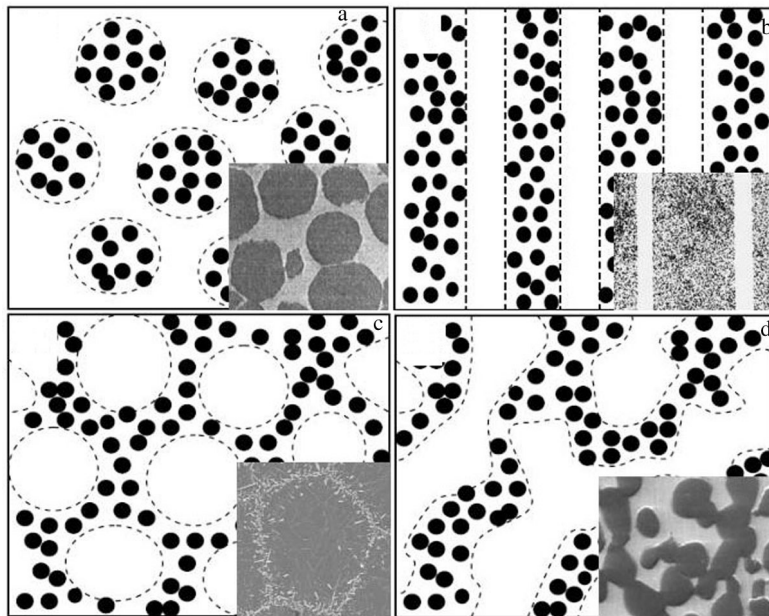


Fig.13 Schematic illustrations and representative SEM images (insets) of microstructural inhomogeneity of a reinforcement-rich phase with four different patterns: (a) isolated, (b) bar/laminated/ring-like, (c) 3D network with isolated particle-lean phase, and (d) 3D network with interconnected particle-lean phase forming the so-called bi-continuous microstructure<sup>[60]</sup>

They found that the increase in the number of dislocation lines was due to the tensile process caused by the dislocation line sliding along the slip plane. Due to a large number of SiC particles, the gaps between the particles were so small that most of the dislocations were difficult to bypass the SiC particles. This in turn hindered their propagation. They gathered near the interface formed by the SiC particles and aluminum matrix, forming a special dislocation source region and generating a large number of new dislocations. Thus, the dislocations were multiplied.

### 3.2.3 Heat mismatch reinforcement mechanism

Different thermal expansion coefficients of the metal matrix and the reinforcing phase lead to different degrees of deformation. Therefore, during deformation and cooling, the interface between the matrix and the reinforcing material will produce strain gradient. The resulting dislocation is called thermal mismatch dislocation, through which the strength of the material can be improved. The formula for the effect of thermal mismatch strengthening proposed by Trojanova et al<sup>[64]</sup> is expressed as follows:

$$\Delta\sigma_{CTE} = \alpha G_m b \sqrt{\rho} \quad (3)$$

where  $\Delta\sigma_{CTE}$  is the thermal expansion coefficient difference between the reinforcing phase and the matrix,  $G_m$  is the shear modulus of the aluminum matrix,  $b$  is the Burgers vector of the dislocation, and  $\alpha$  is the dislocation strengthening efficiency.

### 3.2.4 Heterogeneous deformation-induced reinforcement mechanism

The heterogeneous deforming-induced (HDI) reinforcement theory was proposed by Zhu et al<sup>[65]</sup>. Its theoretical model is shown in Fig. 15. In this model, hard and soft phases occur in heterogeneous materials, and the interface between these phases has an important influence on the deformation behavior and mechanical properties of the materials.

In the elastoplastic deformation stage, the soft phase yields first. Since the hard phase is still in the elastic deformation state, the packing geometry on the soft phase side of the interface must be dislocated to form the strain gradient and maintain the strain continuity. When both phases enter the

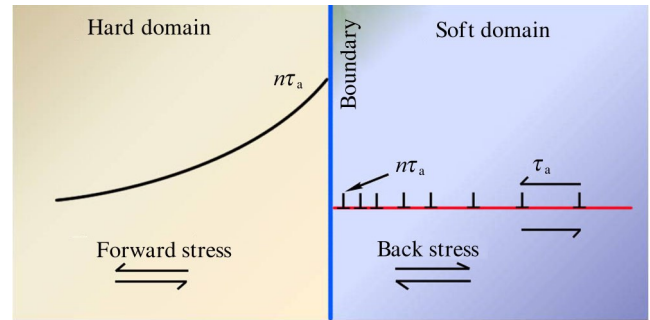


Fig. 15 Theoretical model schematics of hetero-deformation-induced strengthening and processing hardening<sup>[65]</sup>

plastic deformation, a strain gradient must be located near the interface to adapt to the strain partition since the soft phase has endured a greater plastic deformation than the hard phase. The strain gradient should be adjusted by geometrically necessary dislocations to generate metamorphosis-induced hardening, which helps maintain its plasticity.

Unlike other reinforcement mechanisms, the physical origin of HDI strengthening is due to the ability of geometrically necessary dislocations to insert into the heterogeneous interface. This adds additional work-hardening capacity to the material while improving material strength and plasticity. Thus, using and exerting HDI to strengthen metallic materials has become a new, important means for strengthening and toughening non-uniform materials.

Among the above-mentioned strengthening and toughening mechanisms, HDI strengthening has attracted much attention. This mechanism utilizes the superiority of the composite material's soft and hard phases during deformation, which allows the aluminum substrate to undertake the main strain of the soft phase while the reinforcing particles assume the main stress. Because strain and stress are formed within the material due to its uneven distribution, a comprehensive performance with excellent strength and plasticity is obtained.

## 4 Technical Difficulties in Preparing SiC<sub>p</sub>/Al Composites

### 4.1 Mutual wettability of SiC<sub>p</sub>/Al composites

The interfacial tension and tension equation of solid-liquid-gas three-phase contact surfaces were first proposed by Young<sup>[66]</sup>. This equation, often called the Young equation or contact angle equation, is shown in Eq.(4). It is also known as the wetting equation, as it describes the boundary condition of the wetting phenomenon. The smaller the contact angle, the better the wettability. Generally, the boundary is 90°, and a contact angle  $\theta > 90^\circ$  is called non-wetting, while a surface with  $\theta > 135^\circ$  is usually called a super hydrophobic surface. When  $\theta < 90^\circ$ , it is wetted. When  $\theta = 0^\circ$  or there is no equilibrium contact angle, completely spontaneous wetting occurs.

$$\cos \theta = \frac{\gamma_{sg} - \gamma_{sl}}{\gamma_{lg}} \quad (4)$$

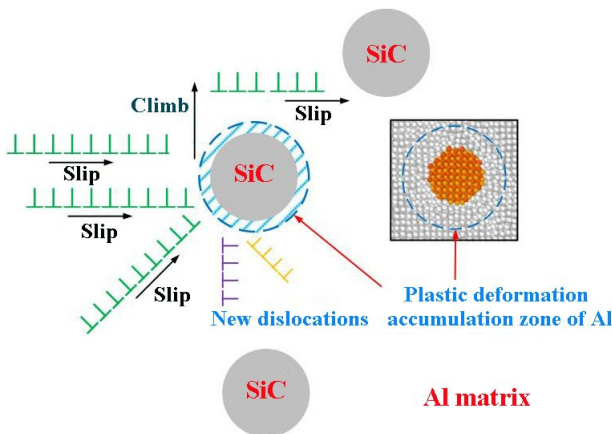


Fig. 14 Schematic of Orowan strengthening mechanism showing dislocation propagation and multiplication<sup>[63]</sup>

Wang et al.<sup>[67]</sup> studied the Al-12Si-1.5Mg-4Ti foil in vacuum brazing of high-volume fraction SiC<sub>p</sub>/Al composites. They found that Ni and Ti coatings had a significant effect on the wettability of the filler metal and the composite, in which the intermetallic compound Ti(AlSi)<sub>3</sub> existed in the weld as an in-situ reinforcing phase. The three phases of solid, liquid, and gas and their contact angles are shown in Fig. 16. The SiC particles are used as the solid phase, and liquid aluminum is used as the liquid phase to analyze the wetting characteristics.  $\gamma_{sl}$ ,  $\gamma_{sg}$ , and  $\gamma_{lg}$  represent the solid-liquid interfacial tension, solid-gas interfacial tension, and liquid-gas interfacial tension, respectively.  $\theta$  is the contact angle.

Generally, the wettability of the SiC particles and Al alloy matrix is poor, and it is difficult to create a composite with conventional methods. Therefore, solving the wettability problem has become a key factor for preparing SiC<sub>p</sub>/Al composites with a uniform distribution of SiC particles, good interface bonding, and excellent comprehensive properties. According to Young's equation, good wettability can be obtained only when the wetting angle  $\theta$  is reduced. Therefore, the basic methods to improve wettability are as follows: (1) increasing the particle surface energy  $\gamma_{sg}$ , (2) reducing the melt surface tension  $\gamma_{lg}$ , and (3) reducing the interface energy between the particles and the melt metal  $\gamma_{sl}$ .

#### 4.2 Interface reaction between SiC particles and Al

The interface between the matrix and the reinforcement is a phase with a certain thickness (above 1 nm). Since the structures of the matrix and reinforcement are different, the interface acts as the link between them that transmits stress and other information. Various interfacial reactions may occur when composites are prepared at high temperatures<sup>[68, 69]</sup>. These interfacial reactions are directly related to the bonding of interfaces and thus affect the composites' properties. The interfacial bonding of composites can be roughly divided into the following categories: physical bonding, diffusion bonding, and chemical bonding.

Researchers<sup>[70-75]</sup> prepared SiC<sub>p</sub>/Al composites using different alloy compositions and pretreated or untreated particles. Some researchers used thermodynamic analysis of the reaction interface to determine the relationship between the free initiation and temperature of the reaction process.

The preparation process, technological parameters, and

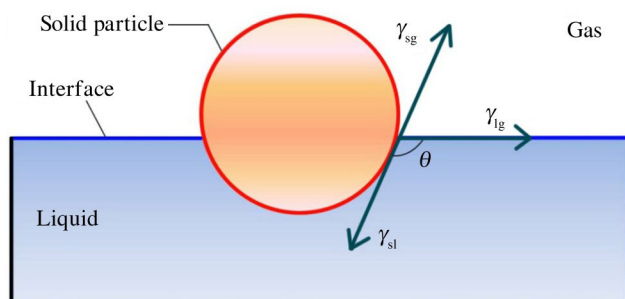


Fig.16 Schematic diagram showing the contact angle formed between the solid, liquid, and gas phases<sup>[67]</sup>

other factors have a great influence on the interface reaction. For example, Mg, Si, and other elements in the matrix inhibit the formation of the Al<sub>4</sub>C<sub>3</sub> brittle phase<sup>[70]</sup>, which can reduce the interface reaction and strengthen the interface between the matrix and the reinforcement. The wettability of the SiC particles and matrix can be improved by the formation of SiO<sub>2</sub> layer on the surface of the reinforced SiC particles after sintering at high temperature<sup>[71]</sup>. External factors, such as temperature and cooling rate<sup>[72]</sup>, also have a certain influence on the interface reaction.

Therefore, the following effective measures can be taken into account to improve interface bonding: (1) Mg, Si, and other elements can be added to the alloy liquid, and the appropriate matrix strength can be selected<sup>[73]</sup>; (2) either HF acid cleaning, preheating, and sintering of the SiC particles or coating the surface of the SiC particles can be performed, and the appropriate particle size can be selected<sup>[74]</sup>; (3) the appropriate secondary processing technology, such as equal channel angular pressing (ECAP), can be chosen<sup>[75,76]</sup>.

## 5 Summary and Prospects

At present, the preparation methods for SiC<sub>p</sub>/Al composites have not been perfected, and the powder metallurgy method is hard to meet the requirements of size and precision. Furthermore, the production cost of this method is still very high. Thus, industrial production must be studied to improve the yield rate and output, and to realize industrial mass production of SiC<sub>p</sub>/Al composites.

Research on the interface behavior between SiC particles and the matrix, as well as the strengthening mechanism for SiC/Al composites is not complete, rendering control of the interface reaction of SiC<sub>p</sub>/Al composites is imprecise. Future research should focus on the preparation process, matrix alloy composition, interface behavior of SiC<sub>p</sub>/Al, and surface condition of SiC particles.

Additionally, the distribution uniformity of SiC particles in the matrix is not well controlled. When the volume fraction of micro- and nano-SiC particles reaches a certain value, serious agglomeration phenomena occur. Few reports on nano-SiC/Al composites exist relatively. Therefore, further research on nano-SiC/Al composites should be the focus in this field.

A large number of basic studies have examined in terms of the microstructure, mechanical properties, and fracture characteristics of SiC<sub>p</sub>/Al composites and have realized the organic combination of experimental research, physical models, and numerical simulation analysis. Moreover, the key factors restricting the development of these composites are gradually eliminated, so their application is extensive and diversified. Future research will be able to overcome the outstanding interface problems and realize controllability of the uniform distribution of SiC particles in the matrix.

## References

- 1 Ibrahim I A, Mohamed F A, Lavernia E J. *Journal of Materials Science* [J], 1991, 26 (5): 1137

- 2 Qi Y S, Wang Y B, Du L J et al. *Rare Metal Materials and Engineering*[J], 2020, 49(11): 3741
- 3 Jiang H, Wang F, Li X et al. *Rare Metal Materials and Engineering*[J], 2021, 50(1): 349 (in Chinese)
- 4 Xu F M, Zhao J, Wang F G. *Journal of Materials Science Letters* [J], 2003, 22: 899
- 5 Song M, Huang B Y. *Materials Science and Engineering A*[J], 2008, 488: 601
- 6 Huang S T, Yu X L. *The International Journal of Advanced Manufacturing Technology* [J], 2018, 94: 3633
- 7 Myriounis D P, Hasan S T, Matikas T E. *Composite Interfaces* [J], 2010(17): 347
- 8 Zhong Z W, Lin G. *The International Journal of Advanced Manufacturing Technology* [J], 2006, 27:1077
- 9 Zhang Y, Yan J C, Wu Q. *Journal of Materials Science and Technology* [J], 2009, 25(3): 378
- 10 Teng X Y, Chen W Q, Huo D H et al. *Composite Structures*[J], 2018(203): 636
- 11 Shetly N, Shahabaz S M, Sharma S S et al. *Composite Structures* [J], 2017(176): 790
- 12 Nicholls C J, Boswell B, Davies et al. *The International Journal of Advanced Manufacturing Technology*[J], 2016(90): 2429
- 13 Chawla N, Chawla K K. *Journal of Materials Science*[J], 2006 (41): 913
- 14 Shankar S, Balaji A, Kawin N. *Particulate Science and Technology*[J], 2018, 36(6): 762
- 15 Huo H W, Woo K D, Guo G S et al. *Journal of Materials Science* [J], 2007, 42: 59
- 16 Myriounis D P, Hasan S T, Matikas T E. *Composite Interfaces* [J], 2008, 15(5): 495
- 17 Kim C S, Cuo K, Manjili M H et al. *Journal of Materials Science* [J], 2017, 52: 13 319
- 18 Chen Yaxi, Guan Lina, Liu Chunqiu. *Journal of Anhui Polytechnic University*[J], 2020, 35(5): 12 (in Chinese)
- 19 Zhang Fulong, Liang Xiaowen. *Bulletin of the Chinese Ceramic Society*[J], 2021, 40(3): 984 (in Chinese)
- 20 Yan H, Rao Y S, He R. *Journal of Materials Processing Technology*[J], 2014, 214(3): 612
- 21 Guan L N, Geng L, Zhang H W et al. *Transactions of Nonferrous Metals Society of China*[J], 2011, 21(2): 274
- 22 Xie K B, Wang X J, Wu K et al. *Materials Science and Engineering A*[J], 2011, 528(29-30): 8709
- 23 Wang L, Qiu F, Zou Q et al. *Materials Characterization*[J], 2017, 131: 195
- 24 Xie K B, Wang X J, Wu K et al. *Journal of Alloys and Compounds*[J], 2017, 509(35): 8664
- 25 Zhang H W, Geng L, Guan L N et al. *Materials Science and Engineering A*[J], 2010, 528(1): 513
- 26 Liao J H, Chen Z F, Guan T Z et al. *Materials Science and Engineering A*[J], 2021, 811: 141 051
- 27 Yang H R, Kwon H, Lee K B. *Materials Science and Technology* [J], 2011, 27(6): 1053
- 28 Sun Z M, Hu X S, Wang X J et al. *Composites Communications* [J], 2021(24): 100 640
- 29 Zhang W X, Lin B, Tang Yet al. *Ceramics International*[J], 2021, 47(12): 16 891
- 30 Maleki K, Alizadeh A, Hajizamani M. *Ceramics International* [J], 2021, 47(2): 2406
- 31 Karan, Pachauri P, Kumar A et al. *Materials Today: Proceedings* [J], 2021, 47(13): 4026
- 32 Zegeye D B, Sinha D K, Venkatesh C et al. *Materials Today: Proceedings*[J], 2021, 47(13): 3811
- 33 Purusothaman M, Rajesh S, Chokkalingam R. *Materials Today: Proceedings* [J], 2021, 45: 6907
- 34 Yang M J, Zhang D M, Gu X F et al. *Journal of Materials Science* [J], 2005, 40(18): 5029
- 35 Maizza G, Mastrorillo G D, Grasso S et al. *Journal of Materials Science* [J], 2017, 52(17): 10 341
- 36 Logsdon W A, Liaw P K. *Engineering Fracture Mechanics*[J], 1986, 24(5): 737
- 37 Xiang J F, Xie L J, Hu X et al. *Rare Metal Materials and Engineering*[J], 2019, 48(5): 1687 (in Chinese)
- 38 Kang C G, Youn S W. *Journal of Materials Processing Technology* [J], 2004, 147: 10
- 39 Bao Y J, Zhu X C, Lu S X et al. *Rare Metal Materials and Engineering*[J], 2021, 50(3): 1084 (in Chinese)
- 40 Alaneme K K. *The West Indian Journal of Engineering*[J], 2013, 35(2): 31
- 41 Arivukkarakasana S, Dhanalakshmi V, Stalin B et al. *Particulate Science and Technology*[J], 2018, 36(8): 967
- 42 Myriounis D P, Matikas T E, Hasan S T. *Strain: An International Journal for Experimental Mechanics*[J], 2012, 48: 333
- 43 Chapmann, Silvaj, Williamsjj et al. *Materials Science and Technology* [J], 2015, 31(5): 573
- 44 Varolt, Canackia, Ozkayas et al. *Particulate Science and Technology*[J], 2018, 36(3): 312
- 45 Alizadeh M, Paydar M H. *Journal of Alloys and Compounds*[J], 2010, 492(1-2): 231
- 46 Sahin Y, Acllar M. *Composites Part A: Applied Science & Manufacturing*[J], 2003, 34(8): 709
- 47 Mao A N, Dun Y P, Lin J M. *Foundry*[J], 2020, 69(3): 228 (in Chinese)
- 48 Bai Yuelong, Zhang Zhifeng, Fan Jianzhong. *Special Casting and Nonferrous Alloys*[J], 2021, 41(4): 402 (in Chinese)
- 49 Buir T, Ouellet, Kocefe D. *Metallurgical and Materials Transactions B*[J], 1994, 25: 607
- 50 Gao Wenli, Su Hai, Zhang Hui et al. *Transactions of Nonferrous Metals Society of China*[J], 2010, 20(1): 49
- 51 Sun Youping, Yan Hongge, Chen Gang et al. *Special Casting Nonferrous Alloys*[J], 2010, 30(8): 691 (in Chinese)
- 52 He Yiqiang, Zhou Haisheng, Li Junjie et al. *Journal of Plasticity Engineering* [J], 2015, 22(6): 152 (in Chinese)

- 53 Ding Zhanlai, Fan Yunchang, Qi Haibo et al. *Transactions of Nonferrous Metals Society of China*[J], 1999(9): 265
- 54 Tokaji K, Shiota H, Kobayashi K. *Fatigue and Fracture of Engineering Materials and Structures*[J], 1999(22): 281
- 55 Wang Y F, Liao W H, Yang K et al. *International Journal of Advanced Manufacturing Technology*[J], 2019, 100(1-4): 963
- 56 Wang T, Xie L J, Wang X B. *The International Journal of Advanced Manufacturing Technology*[J], 2015, 79: 1185
- 57 Han J J, Hao Q X, Li L et al. *The International Journal of Advanced Manufacturing Technology*[J], 2017, 92: 1875
- 58 Bian R, He N, Li L et al. *The International Journal of Advanced Manufacturing Technology*[J], 2014, 71: 411
- 59 Dong Z G, Zheng F F, Zhu X L et al. *The International Journal of Advanced Manufacturing Technology*[J], 2017, 93: 2827
- 60 Huang L J, Geng L, Peng H X. *Progress in Materials Science* [J], 2015, 71: 93
- 61 Hansen N. *Scripta Materialia* [J], 2004, 51(8): 801
- 62 Wu G Q, Zhang Q Q, Yang X et al. *Composite Interfaces*[J], 2014, 21(5): 415
- 63 Huo S Y, Xie L J, Xiang J F et al. *Applied Physics A*[J], 2018, 124(2): 209
- 64 Trojanova Z, Pahutova M, Kiehn J. *Key Engineering Materials* [J], 1997, 127(131): 1001
- 65 Zhu Y T, Wu X L. *Materials Research Letters*[J], 2019, 7(10): 393
- 66 Young T. *Philosophical Transactions of the Royal Society*[J], 1805, 95: 65
- 67 Wang P, Xu D X, Cheng D F et al. *Science and Technology of Welding and Joining* [J], 2015, 20(5): 361
- 68 Ferro A C, Derby B. *Acta Metallurgica et Materialia*[J], 1995, 43(8): 3061
- 69 Lee J C, Ahn J P, Shim J H et al. *Scripta Materialia*[J], 1999, 41(8): 895
- 70 King L B, Liu Y L, Nyberg E et al. *Composites Science and Technology*[J], 1992, 43(1): 85
- 71 Lee J C, Ahn J P, Shi Z L et al. *Metallurgical and Materials Transactions A*[J], 2001, 32(6): 1541
- 72 Wang A Q, Liu P, Xie J P et al. *Composite Interfaces*[J], 2015, 22(9): 847
- 73 Mandal D, Viswanathan S. *Materials Characterization*[J], 2013, 85: 73
- 74 Ghosh S, Moorthy S. *Acta Materialia* [J], 1998, 46(3): 965
- 75 Mohsenih, Keirs S, Chans L I et al. *Materials Science and Technology*[J], 2010, 26(5): 597
- 76 Bonora N, Ruggiero A. *Composites Science & Technology*[J], 2006, 66(2): 314

## SiC 颗粒增强铝基复合材料的制备技术及性能研究进展

王运雷<sup>1,2,3</sup>, 任莉平<sup>1</sup>, 杨方洲<sup>1</sup>, 刘奇<sup>2</sup>, 曹宇<sup>3</sup>, 罗宏伟<sup>4</sup>

(1. 重庆文理学院 材料科学与工程学院, 重庆 402160)

(2. 重庆材料研究院有限公司 国家仪表功能材料工程技术研究中心, 重庆 400707)

(3. 重庆大学 材料科学与工程学院, 重庆 400044)

(4. 重庆柏锐柯新材料科技有限公司 技术研发部, 重庆 402560)

**摘要:** SiC 颗粒增强铝基复合材料具有高的比强度、高的比模量、高的耐磨性以及优异的抗腐蚀性能, 在机械结构轻量化设计方面是替换传统钢铁的最佳选择材料之一, 在汽车、机械、航空及电子封装等领域具有广阔的应用前景。因此, 备受各界科研工作者的关注。对 SiC 颗粒增强铝基复合材料的制备方法、性能、强化机制进行了归纳总结, 分析并探讨了 SiC/Al 复合材料的制备技术难点及改进方法, 最后对 SiC/Al 复合材料的研究及应用进行了总结与展望。

**关键词:** SiC 颗粒; 铝基复合材料; 制备技术; 强化机制

作者简介: 王运雷, 男, 1985 年生, 博士, 讲师, 重庆文理学院材料科学与工程学院, 重庆 402160, 电话: 023-49855073, E-mail: wangyunlei@cqu.edu.cn